SEISMIC EVENT DISCRIMINATION USING TWO-DIMENSIONAL GRIDS OF REGIONAL P/S SPECTRAL RATIOS: APPLICATIONS TO NOVAYA ZEMLYA AND THE KOREAN PENINSULA

Mark D. Fisk[1], Steven R. Taylor[2], William R. Walter[3], and George E. Randall[4]
Alliant Techsystems[1], Rocky Mountain Geophysics, LLC[2], Lawrence Livermore National Laboratory[3], and Los Alamos National Laboratory[4]

Sponsored by the National Nuclear Security Administration

Award Nos. DE-AC52-07NA28116[1,2], LL07-BAA07-46-NDD03[3], LA07-BAA07-46-NDD03[4]
Proposal No. BAA07-46

ABSTRACT

Building upon previous developments for the Semipalatinsk, Lop Nor, and Nevada test sites (Fisk, 2008; Fisk et al., 2008), two-dimensional (2D) grids of P/S (Pn/Sn, Pn/Lg, Pg/Lg) ratios, for all combinations of frequencies of P- and S-wave spectra, are used to enhance seismic event discrimination for the Arctic region, including the Novaya Zemlya test site (NZTS), and for the Yellow Sea and Korean Peninsula (YSKP). The spectra of regional phases are corrected for source size (under the earthquake hypothesis), geometrical spreading, attenuation, and site effects. For the Arctic, data from station KEV are the main focus of the analysis, which is applied to underground nuclear tests (UNTs) at NZTS, peaceful nuclear explosions (PNEs) in the former Soviet Union, underwater explosions, and earthquakes. The relative spectra from AMD (Amderma, Russia) recordings of a pair of events in the Kara Sea on 16 August 1997 are modeled to estimate stress drop. The corrected Pn/Sn grids exhibit prominent evidence of source differences and modulations in both Pn and Sn spectra for various types of explosions. Grid measurements include narrowband (e.g., 6–8 Hz) Pn/Sn and broader-spectral Pn(2.5–9 Hz)/Sn(4-9 Hz) ratio. Due to spectral variations for explosions, the broader-spectral Pn/Sn reduces the variance and increases the mean separation of explosions and earthquakes, improving discrimination over narrowband Pn/Sn. Robustness is examined with respect to the site and source corrections. Kriged path corrections are also computed and applied. Misfits to the correction model are quantified using the root-mean-squared (RMS) of corrected 2D Pn/Sn grids and a ratio of off-diagonal grid elements. ARCES data illustrate the potential utility of broad spectral features to investigate events. P/S grids and discrimination results are also computed using NORSAR data for 17 UNTs and 9 other nearby events. For the YSKP region, openly available data from stations MDJ in China and TJN in South Korea are used, *á la* Kim and Richards (2007), Koper et al. (2008), and Walter et al. (2007, 2008). The spectral processing and discriminant analyses are applied to earthquakes, mining blasts, and the UNTs in North Korea on 9 October 2006 and 25 May 2009. Grid measurements tested as discriminants include traditional Pg/Lg and Pn/Lg ratios in the 6-8 Hz band, and means, quartiles, RMS values, fractional pixel counts, and others over broader frequencies, e.g., Pn(1–9 Hz)/Lg(0.3–9 Hz). Because there are only two UNTs, mining blasts are included as surrogates for contained explosions; the former generally provide a conservative bound on discrimination performance. The effectiveness of Pg/Lg and Pn/Lg is discussed. Performance is compared using vertical- and three-component (3C) seismic data, and correcting for source size using reported magnitudes or from simultaneous model fits of single-station Pn, Pg, and Lg spectra to estimate M_W. Using 3C data and the model fits both improve discrimination performance. Multivariate discrimination tests are applied to assess the benefit of combining multiple features of the grids. Source model predictions are compared to spectra of regional seismic phases from the UNTs in North Korea. As a separate study (Taylor, 2009), rock damage is investigated as a possible mechanism to explain differences in apparent corner frequencies of explosion P and S waves.

OBJECTIVES

The main objective is to develop and test enhanced discrimination procedures and comparisons to source models, using characteristics of multi-dimensional spectral ratios for regional seismic phases. Fisk (2008) and Fisk et al. (2008) presented two-dimensional (2D) grids of P/S spectral ratios for all combinations of frequencies of P and S wave spectra, that exhibit greater differences in relative spectral amplitudes and shapes between explosions and earthquakes than considered before. Fisk (2008) describes the processing and discrimination methods, and applications to earthquakes and explosions at the Semipalatinsk Test Site (STS), the Lop Nor Test Site (LNTS), and the Nevada Test Site (NTS). Measurements on the 2D grids included traditional narrowband P/S discriminants, cross-spectral P/S ratios, and a root-mean-squared (RMS) misfit to the correction model, under the hypothesis of a Brune (1970) earthquake source. For granite test sites, cross-spectral P/S ratios, using higher frequencies (>2 Hz) of Pn and lower frequencies (<1 Hz) of Sn or Lg, significantly improve discrimination performance over using traditional narrowband P/S measurements. The performance for explosions in porous rock (e.g., at NTS) is much more variable. Fisk (2008) compared the grids and P/S discriminants to model predictions for events at STS, LNTS, and NTS. He also compared model predictions to Pg and Lg spectra and their ratio for the UNT in North Korea on 9 October 2006. He further used model calculations to predict P/S discriminant values for STS, to help substantiate the results and extrapolate how certain discriminants are expected to perform under a broader range of conditions. Here we assess the utility of 2D P/S grids and various spectral measurements for (1) the Arctic region, including NZTS and (2) the Korean Peninsula.

RESEARCH ACCOMPLISHED

Arctic Region

Enhancing discrimination for NZ is especially difficult due to (1) the relative aseismicity of the area; (2) limited ground truth; (3) different times at which seismic stations were installed; (4) limited recordings at regional distances for events at or near NZTS, particularly small events since the moratorium on nuclear weapons testing; and (5) bandwidth limitations due to Nyquist frequencies and noise effects. We focus largely on KEV (Kevo, Finland) data for seismic events over a broad Arctic region. We correct the Pn and Sn spectra for source, geometrical spreading, attenuation, and site effects, and apply the analysis to UNTs at NZTS, peaceful nuclear explosions (PNEs) in the former Soviet Union, several underwater explosions, and regional earthquakes. The grids for the explosions – particularly those underwater, but also many UNTs and PNEs – exhibit clear spectral scalloping. We consider a preliminary set of measurements on the grids that include traditional Pn/Sn discriminants in the 4–6 Hz and 6–8 Hz bands and a broader-spectral Pn/Sn ratio. We also examine path variations for the greater Arctic region and show that their treatment improves discrimination. We further quantify misfits to the correction model, under the hypothesis of a Brune earthquake source, and examine robustness to potential errors in the source and site terms, and to alternate frequency-dependent weighting schemes. We apply the discrimination criteria to several small events near NZ since 2003. Additional analyses performed by Fisk (2009), but not shown here, include (1) modeling relative spectra from AMD (Amderma, Russia) recordings of a pair of events in the Kara Sea on 16 August 1997 to estimate stress drop; (2) investigation of ARCES data; and (3) assessment of P/S grids and discrimination results using NORSAR data for 17 UNTs and 9 nearby events. Although these latter seismic recordings are at distances greater than 20 degrees, their broad spectral characteristics provide compelling evidence of source type.

Figure 1 shows locations of events recorded by ARCES, NORES, NORSAR arrays, station KEV, and/or AMD. Ground-truth source types of many of the events have been published. These events include 12 underground nuclear explosions (peaceful and weapons tests), 56 mining blasts, 5 in-water explosions (including the Kursk accident), 62 earthquakes, and 2 mining-induced tremors on the Kola Peninsula. For purposes of developing discrimination criteria that may be applied to any of the events near NZ since 1992, data from KEV and/or ARCES must be utilized. Most NZTS UNTs were conducted prior to installation ARCES and KEV; they recorded only 3 and 6 UNTs (mb 5.5 to 5.8) from 1982 to 1990. Recordings are also available for 11 other events near NZ from 1992 to 2007, all of which were mb 3.5 or smaller. Ocean-induced seismic noise is high at frequencies below 2–3 Hz at these stations.

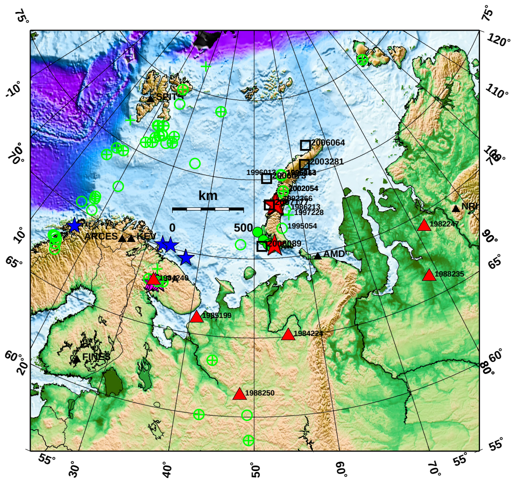

Figure 1. Locations of UNTs (red stars), PNEs (red triangles), mining blasts (magenta stars), in-water explosions (blue stars), and other events. The squares depict events near NZ since 2003.

Figure 2 shows corrected Pn/Sn grids from KEV data for four events (mb ð 3.5) near NZ. Figure 3 shows the grids for four explosions (three underground and one in the Barents Sea. Grids for the underground explosions exhibit similar features as for UNTs at other hardrock test sites, including high cross-spectral Pn/Sn ratios for lower frequencies (e.g., less than 0.5-1.0 Hz) of Sn. Note that the grids for the smaller NZ events (Figure 2) have less usable bandwidth due to low-frequency noise in this region. Although cross-spectral P/S ratios may, in principle, provide better discrimination for NZTS, as for STS and LNTS, SNR limits their utility for small events near NZTS. Note, however, that the grids in Figure 3 illustrate that there are better discriminants to use than traditional narrowband (4–6 Hz or 6–8 Hz) Pn/Sn. The grids for in-water explosions (e.g., bottom right plot of Figure 3) have high Pn/Sn ratios and spectral scalloping at similar frequencies for both Pn and Sn, indicative of water column reverberations and bubble-pulse effects near the source that are imparted to all seismic phases. The grids for many of the PNEs and UNTs (most were salvos) also exhibit spectral scalloping.

Fisk (2008) and Fisk et al. (2008) define criteria using two hypothesis tests, based on the t-distribution, to assess whether an event is rejected as belonging to the explosion and/or earthquake populations. Two p-values are computed, i.e., with respect to each population, giving statistically well-defined criteria to reject or not reject each hypothesis, clear definition of *undetermined*, and flexibility to choose different criteria with respect to different event types, if desired. In the following applications, the significance level is $\alpha = 0.01$. Events rejected by one test and accepted by the other are categorized as the latter event type. Events rejected or accepted by both tests are categorized as *undetermined*. (This category can be split, if desired.) Results based on KEV data for 22 explosions and 37 earthquakes are shown here.

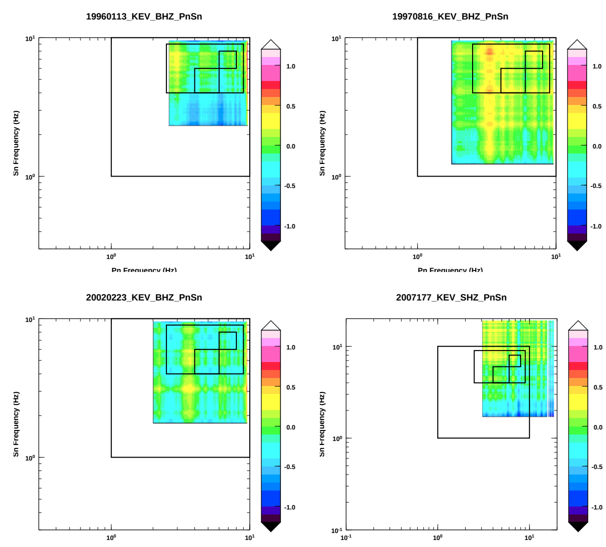

Figure 2. Corrected Pn/Sn 2D spectral ratios from KEV data for four events near NZTS since 1996.

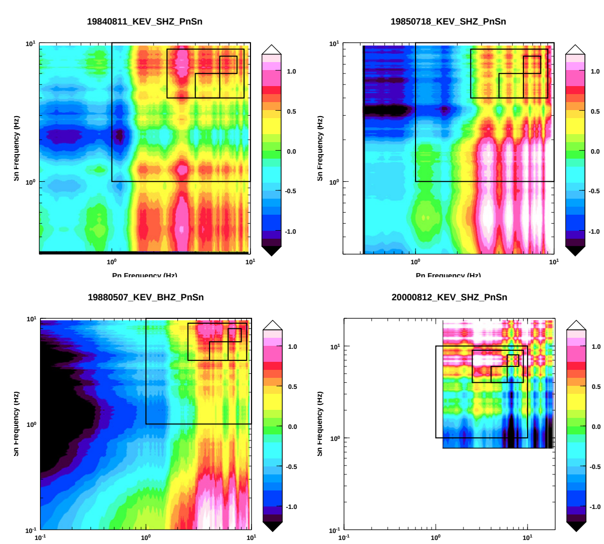

Figure 3. Corrected Pn/Sn 2D spectral ratios, based on KEV recordings of two PNEs (top), an NZTS UNT (bottom left), and the Kursk accident.

Using log Pn/Sn(4-6 Hz), 68% of explosions and 51% of earthquakes are categorized properly. The others are *undetermined*. Using log Pn/Sn(6-8 Hz), 82% and 84% are categorized properly. Figure 4 shows results using a broad-spectral mean of log Pn(2.5-9 Hz)/Sn(4-9 Hz). In this case, 96% and 97% are categorized properly. One PNE and an earthquake are *undetermined*. Progressive improvements for these three Pn/Sn discriminants are due largely to progressive reductions in the variance of the explosion population. Of four events near NZ since 2003 that have KEV data (triangles in Figure 4), three are categorized as *earthquake-like*. The event on jdate 2006073 is *undetermined* using Pn/Sn in the 4-6 Hz or 6-8 Hz bands and also, marginally, using Pn(2.5-9 Hz)/Sn(4-9 Hz), mainly because SNR is low for this event.

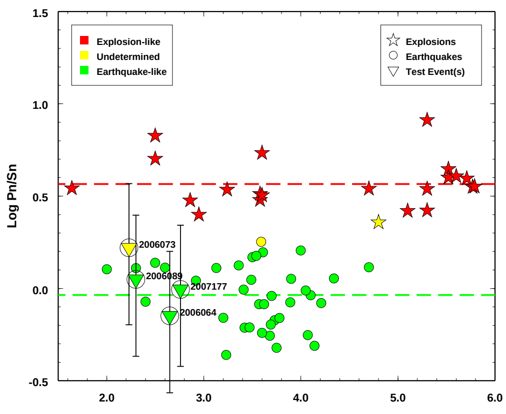

Figure 4. Discrimination results using log Pn(2.5-9 Hz)/Sn(4-9 Hz) measurements from KEV data. The triangles represent four events near NZ since 2006.

Figure 5 shows RMS-misfit versus broad-spectral Pn/Sn values, indicating that all events near NZ since 1995 (large circles) are inconsistent with explosions and consistent with earthquakes, either just near NZ (larger circles and stars) or for the broad Arctic region. The cyan triangles correspond to the various assumed magnitudes used to correct the spectra for an earthquake. The magenta triangles show hypothetical values for the UNT. The RMS-misfit becomes much higher as magnitude is underestimated, particularly for the earthquake. The mean broad-spectral ratio is much less sensitive. The RMS-misfit is a useful indicator of spectra that are inconsistent with the correction model, due to source type or various correction parameters. Figure 5 illustrates that if the corrections are sufficiently inaccurate, an earthquake could be miscategorized as an explosion. The test case shown here indicates that the source parameters would have to be very inaccurate for this to occur. Another grid measurement that particularly highlights errors in source parameters (magnitude or stress drop) is a ratio of the grid values along off-diagonal portions (i.e., a ratio of P/S grid values in the northwest to southeast quadrants).

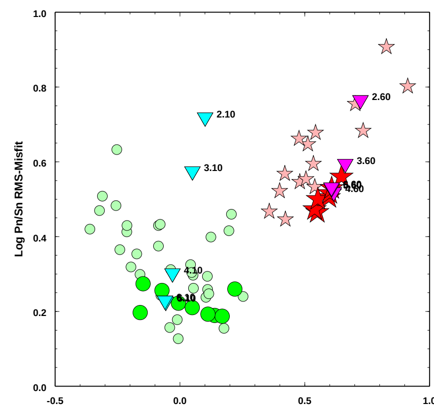

Figure 5. RMS-misfit versus broad-spectral log Pn/Sn values for explosions (stars) and earthquakes (circles). The cyan and magenta triangles are values corresponding to various assumed magnitudes used to correct the spectra for an earthquake and a UNT.

Fisk (2009) also found that the discrimination results are robust to site corrections. It is interesting to assess the impact of path effects, including overall improvements in performance and whether worse performance of Pn/Sn(6-8 Hz), compared to the broad-spectral Pn/Sn, is ameliorated by treating path effects. We use a kriging method (e.g., Fisk and McCartor, 2008) to estimate path corrections as the local Bayesian mean of earthquake data, along with associated uncertainties. For example, Figure 6 shows the spatially-varying mean for the broad-spectral Pn/Sn, showing that there are indeed systematic path variations that can be treated by kriging or another spatial interpolation method. Because the earthquake variance is reduced by kriging path corrections, the significance level can be reduced from 0.01 to 0.005 (99.5% confidence), while achieving comparable discrimination results as without kriging. Using Pn/Sn (6-8 Hz), 77% of the explosions and 88% of the earthquakes are categorized properly. Using Pn(2.5-9 Hz)/Sn(4-9 Hz), 100% of the explosions and 95% of the earthquakes are categorized properly. Considering the increase in assigned confidence level, the performance of both Pn/Sn discriminants improve by applying path corrections. The broad-spectral Pn/Sn discriminant still outperforms Pn/Sn(6-8 Hz).

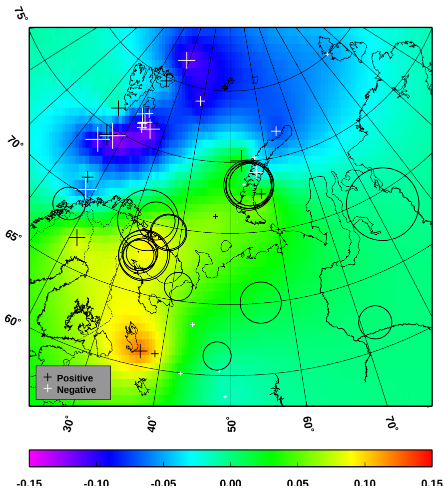

Figure 6. Kriged mean of log[Pn(2.5-9 Hz)/Sn(4-9 Hz)] for KEV, using earthquakes as reference events. Crosses and circles represent earthquakes and explosions. Marker size and color indicate residuals.

Korean Peninsula

We also applied spectral processing and discrimination methods, based on 2D P/S grids, to events in the YSKP region. Figure 7 shows locations of 515 events compiled from various bulletins and publications. Following Kim and Richards (2007), Koper et al. (2008), and Walter et al. (2007, 2008), we used seismic recordings by MDJ in China and TJN in South Korea that are openly available via the IRIS DMC and the Ocean Hemisphere Project Data Management Center (OHPDMC). The stars depict the two UNTs. Bold crosses and circles represent events with recordings from MDJ and TJN, respectively. TJN data are available after 1997. Many TJN and MDJ recordings do not have usable signals for smaller events.The MDJ dataset includes 66 earthquakes, two UNTs, and four small (1-2 ton) chemical explosions conducted in single holes during 1998, part of a refraction survey in China, near the border with North Korea. The TJN dataset includes 38 earthquakes, two UNTs, 25 blasts, and 4 unknown events. (Results for TJN are highlighted here; results for MDJ are comparable.) Figure 8 shows TJN recordings of the UNTs and the nearest earthquake on 2004/12/16, minimizing path differences. Pn/Lg has greater differences between earthquakes and explosions than Pg/Lg. I processed spectra for all three components for MDJ and TJN. I considered cases using 3C data and only the vertical component. As shown by Kim et al. (1997), high-frequency P/S ratios based on 3C data improve discrimination. I corrected the spectra using Q and spreading parameters provided by Walter (2008, pers. comm.). The corrections for source size are based on a Brune model, under the earthquake hypothesis. The form of the corrections is presented by Taylor et al. (2002) and Fisk (2006, 2007), among others. I computed site corrections for Pn, Pg, and Lg at MDJ and TJN by a linear fit of the log spectrum residuals (subtracting the log geometrical spreading, Q, and source terms) versus log frequency for the earthquakes. Figure 9 shows 2D grids of Pn/Lg and Pg/Lg spectral ratios, for all frequencies of P and S wave spectra with adequate SNR, at TJN for the same three events and a mining blast. The top grids have low values, as expected for earthquake spectra that are properly corrected. The grids for the UNTs are quite different, exhibiting similar features as for UNTs at other hard-rock nuclear test sites (cf. Fisk, 2008, 2009). The Pn/Lg grids for the UNTs have higher values than the Pg/Lg grids. The Pg/Lg grid for the mining blast does not deviate as much from zero as the Pn/Lg grid. Modulations are clearly seen in Pn, Pg, and Lg spectra, likely indicative of ripple firing. Modulations observed for multiple phases and/or stations help to confirm that they are due to a (near) source effect.

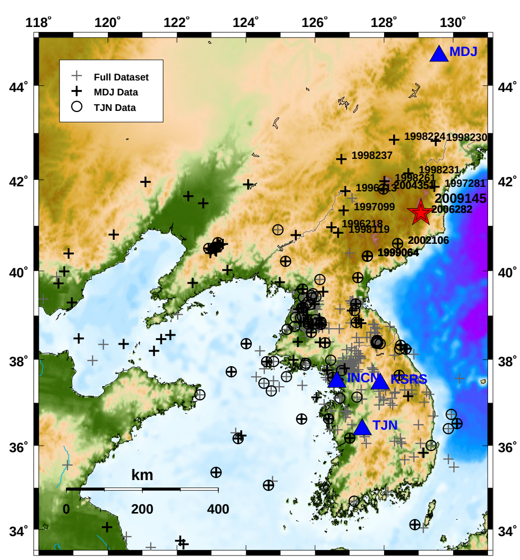

Figure 7. Locations of events and stations. Some events are labeled by Julian date. Black crosses and circles indicate events with data from MDJ and/or TJN, respectively. The stars represent the UNTs.

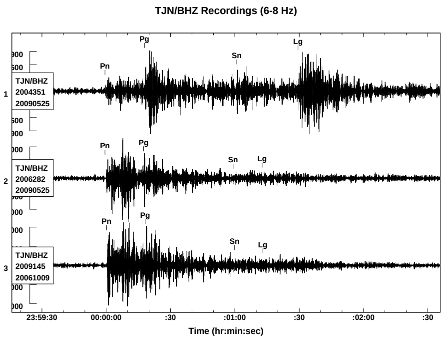

Figure 8. TJN seismograms, filtered in the 6-8 Hz passband, of the 2006 and 2009 UNTs in North Korea and a nearby earthquake on 2004/12/16.

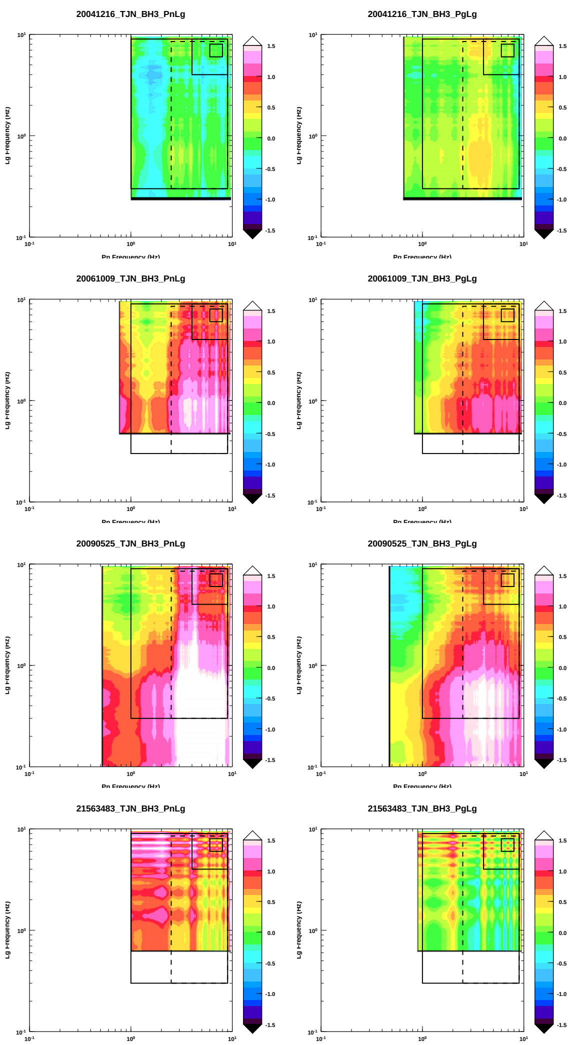

Figure 9. Grids of corrected Pn/Lg (left) and Pg/Lg (right) spectral ratios at TJN for an earthquake, the two UNTs, and a mining blast. The rectangles show spectral bands used to measure various P/S ratios.

Figure 10 shows log Pg/Lg ratios at TJN versus distance in four sets of frequency bands. The top plots show Pg/Lg values in the 4-9 Hz (left) and 6-8 Hz (right) bands. The lower left plot shows mean values using 1.5-9 Hz for Pg and 0.3-9 Hz for Lg. The lower right plot shows RMS values using 1-9 Hz for Pg and 0.3-9 Hz for Lg, intended to quantify the misfit of the correction model to the spectral ratio grid. Pg/Lg values for mining blasts overlap with the earthquakes. Figure 11 shows similar plots of Pn/Lg. There is no significant residual distance dependence for explosions or earthquakes, indicating appropriate corrections. The population variances are larger for Pn/Lg than Pg/Lg discriminants. However, there is also much better separation of the explosion and earthquake populations for Pn/Lg.

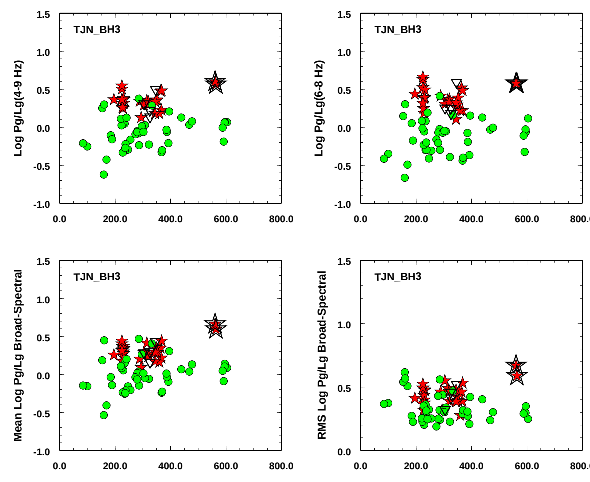

Figure 10. Log Pg/Lg ratios at TJN versus distance for explosions (stars) and earthquakes (circles) in four sets of frequency bands. The two UNTs have the highest values (highlighted stars) in each plot.

The discriminant types and frequency bands shown are a fraction of those tested, including medians, quartiles, minima, maxima, L1 deviations, and variances of the grids in various bands. A new type that discriminates very effectively is a fractional count of pixels above or below high and low thresholds, quantified as the sum of +1 for every pixel with a log Pn/Lg value greater than 0.8 (orange and higher) and –1 for those less than 0.3 (light green and lower), divided by the total number of pixels with adequate signal-to-noise ratio. Conceptually, this quantifies the visual impact of the grids, where ones with mostly high values appear distinct from those with mostly low values. Figure 12 shows these fractional counts of log Pn(1.5-9 Hz)/Lg(0.3-9 Hz) versus distance for TJN and MDJ. They provides the best (complete) separation of all discriminants examined and also lower variance. Further work is needed to formulate the statistics of these measurements for use in hypothesis testing.

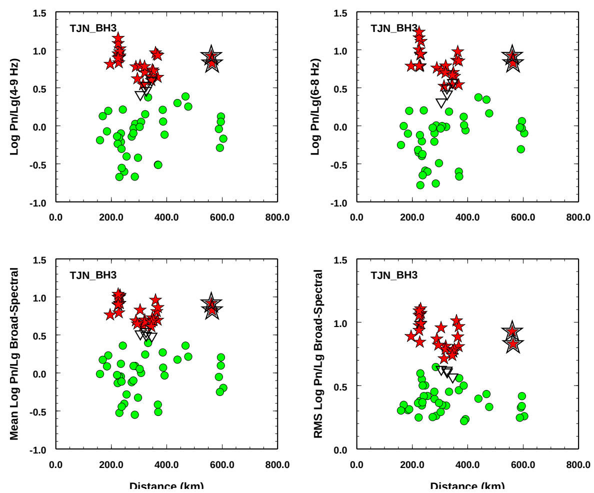

Figure 11. Similar to Figure 10, but for Pn/Lg.

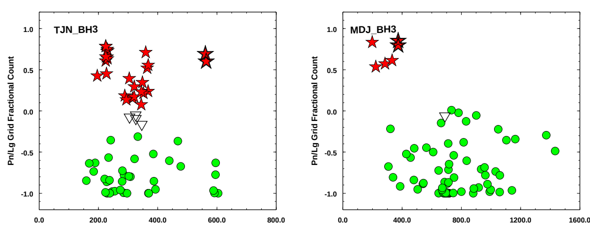

Figure 12. Broad-spectral Pn/Lg fractional grid counts versus distance for TJN and MDJ. It captures visual differences of the grids for earthquakes and explosions, and provides the best discrimination of measurements examined so far.

Figure 13 (top) shows discrimination results for log Pg/Lg(6-8 Hz) using TJN and MDJ 3C data. Only 35% of explosions, including the two UNTs, and 70% of earthquakes are categorized properly. Several types of Pg/Lg measurements and various options were tested, but none performed as well as the Pn/Lg discriminants. Figure 13 (bottom) shows the results for log Pn(1.5-9 Hz)/Lg(1-9 Hz) using from TJN and MDJ 3C data. In this case, 90% of explosions and 96% of earthquakes are categorized properly. Both UNTs are categorized as *explosion-like*. They have p-values with respect to the earthquake population of 0.00032 and 0.000098, i.e., very low probabilities that an earthquake would generate such observations. As found by Fisk (2008, 2009) for other nuclear test sites, there are features of 2D Pn/Lg and Pn/Sn grids that provide better discrimination performance than traditional P/S in the 6-8 Hz band.

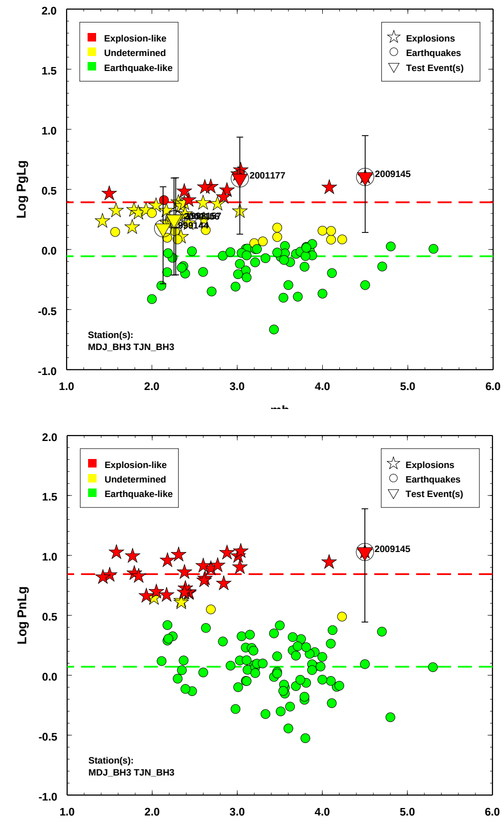

Figure 13. Discrimination results versus magnitude using log Pg/Lg(6-8 Hz) (top) and log Pn(1.5-9 Hz)/Lg(1-9 Hz) (bottom) from TJN and MDJ 3C data. A 99% confidence interval is shown for the 2009/05/25 UNT and selected other events.

I also applied multivariate outlier and discrimination methods, based on generalized likelihood ratios (GLR) and the bootstrap (Fisk et al., 1993), to assess the benefit of combining multiple grid features. I tested the different techniques and various sets of discriminants. Figure 14 shows the result of using three features of the grids: mean Pn/Lg(4-9 Hz), mean Pn(1.5-9 Hz)/Lg(0.3-9 Hz), and RMS Pn(1-9 Hz)/Lg(0.3-9 Hz). Plotted are p-values with respect to the earthquake and explosion populations. All events are categorized properly at 0.01 significance level. As for the univariate cases, the two UNTs are categorized as *explosion-like*. Their p-values with respect to earthquakes indicate very low probabilities that an earthquake would have generated the observations.

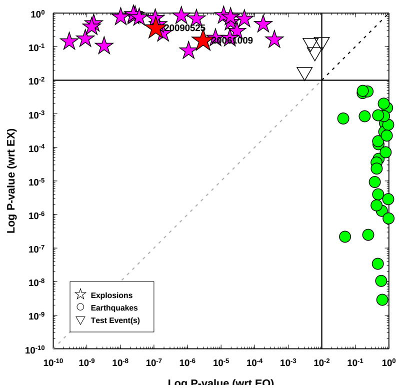

Figure 14. Multivariate results, computed as p-values with respect to earthquake and explosion populations, using 3 Pn/Lg measurements at TJN.

Using kriging (Fisk and McCartor, 2008), Figure 15 shows spatial variations of corrected broadband Pn/Lg at TJN and MDJ. This discriminant, and the others, exhibit systematic path variations for both stations. For TJN, all types of mean Pn/Lg discriminants are systematically lower, on average, for offshore earthquakes. For MDJ, the highest Pn/Lg values are for earthquakes with partial paths to MDJ beneath the Sea of Japan, where water depth is greater than the Yellow Sea (e.g., Figure 15), perhaps indicating stronger attenuation and/or blockage of Lg for such paths. Kriging is not necessary to obtain good discrimination performance, but it is beneficial.

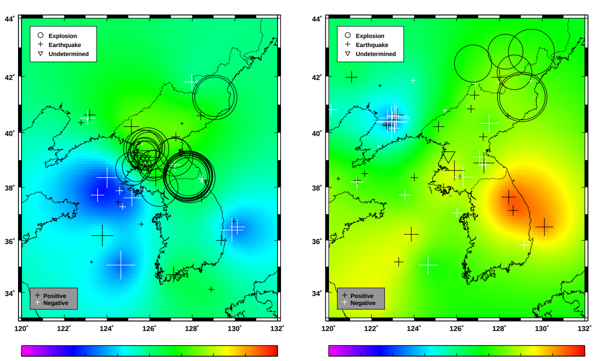

Figure 15. Kriged local mean of broad-spectral Pn/Lg from earthquake data for TJN and MDJ. Circles and crosses represent explosions and earthquakes. Marker size and color indicate the residuals.

Figure 16 shows observed (cf. Walter et al., 2007) and model Pg and Lg spectra (left) and spectral ratios (right) for the 2006/10/09 UNT in North Korea. The model results, using Mueller and Murphy (1971) [MM71] for P waves and with shifted corner frequency for S waves (cf. Fisk, 2006, 2007), compares even better for Lg than Pg, similar to findings by Fisk (2007) for NTS.

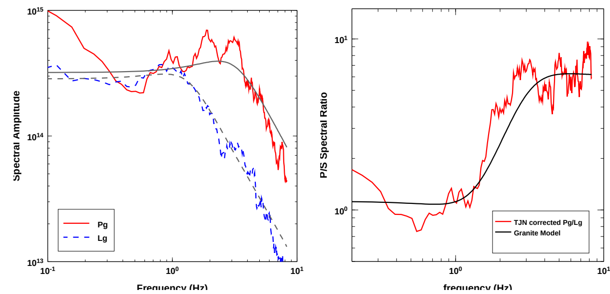

Figure 16. Corrected Pg and Lg spectra (left) and Pg/Lg spectral ratio (right) from the TJN recording of the 2006/10/09 UNT. Also shown are model results.

Rock Damage Mechanics

Taylor (2009) investigated rock damage as a possible mechanism to explain differences in apparent corner frequencies of explosion P and S waves (Xie and Patton, 1999; Fisk, 2006, 2007; Murphy et al., 2009). The main conclusion is that rock damage is a plausible source of explosion S waves and a possible explanation of reduced corner frequencies for S waves, relative to P.

CONCLUSIONS AND RECOMMENDATIONS

Key results for the Arctic region indicate that (1) very good discrimination is obtained; (2) using Pn and Sn measurements over broader spectral ranges is much more stable and informative, improving performance over narrowband P/S discriminants; (3) treatment of systematic path variations improves discrimination; (4) noise effects at frequencies of about 3 Hz and below are very significant for all NZ events since 1992; (5) cross-spectral P/S ratios may provide the best discrimination for NZTS, as for other hardrock test sites, but they have limited utility for available stations and events near NZTS since 1992. To distill the specific discrimination results of Fisk (2009), (1) there does not seem to be any problem identifying NZTS explosions, at least above mb 3.8; (2) the Kara Sea events on 1986/08/01 and 1997/08/16 have spectral features at NORSAR that are consistent with aftershocks during 1973-1974 and inconsistent with known UNTs; (3) all other small events in the vicinity of NZ since 1992 with KEV data have spectral features consistent with the Kara Sea events; (4) the 1992/12/31 event is the most ambiguous event near NZTS; and (5) the 1995/06/13 event, which also does not have KEV data, has very similar Pn/Sn spectral ratios at ARCES over 6–15 Hz, as the 1992/12/31 event. In addition, their spectra are the least consistent with a Brune earthquake source model. With the exception of these latter two events that need further evaluation, the results of Fisk (2009) provide a comprehensive assessment of source types for all events of relevance to monitoring NZTS.

Key results for the YSKP region are as follows. Features of Pn/Lg grids provide very effective discrimination for events with adequate SNR. Overall performance needs to be quantified, including application rates, for stations available for monitoring. Pg/Lg and Pn/Lg from 3C data improves performance over using vertical-component data. Discrimination criteria using multiple Pn/Lg measurements accurately categorize all events in the explosion and earthquake sets. The best discriminant tested is log Pn(1.5–9 Hz)/Lg(0.3–9 Hz), which quantifies the mean deviation of Pn/Lg to the Brune model over broad frequency ranges. The results are not very sensitive to corrections for source size. The Pn/Lg discriminants exhibit path variations with apparent correlation to geophysical features for TJN and MDJ. Discrimination performance is further improved by applying path corrections. The spatial dependence for MDJ suggests that paths beneath the Sea of Japan may extinguish high-frequency Lg. The 2009/05/25 and 2006/10/09 UNTs in North Korea have very similar spectral features and discrimination results. Using broad-spectral log Pn(1.5–9 Hz)/Lg(1–9 Hz) measurements from TJN and MDJ 3C data, the 2009/05/25 UNT is discriminated from earthquakes at a 99.99% confidence level. Smaller variances of Pg/Lg for earthquakes compensate for less separation from earthquakes than Pn/Lg for the two UNTs. However, none of the Pg/Lg discriminants separate small blasts from earthquakes at TJN or MDJ. Thus, many earthquakes and blasts are *undetermined* using Pg/Lg.

Using MM71 for P waves and with a shifted corner frequency for S waves (cf. Fisk, 2006), agrees very well with the spectra at TJN for the 2006/10/09 UNT. The apparent corner frequency for Lg is lower than that of Pg, which explains the same frequency dependence of P/S spectral ratios for UNTs at all test sites examined (STS, LNTS, NZTS, and test sites in India and North Korea). Walter et al. (2007) showed a model calculation, using a P-to-S transfer function, that also represents the Lg spectrum very well for the 2006 UNT. P-to-S conversion, as well as near source effects are plausible mechanisms to generate S waves from explosions. Many important physical effects need further study.

In summary, the results of the studies for STS, LNTS, NTS, NZTS, and the North Korean test site indicate (1) there are features of the P/S spectral ratio grids over broader spectral ranges that significantly improve performance relative to traditional P/S discriminants; (2) the results are robust to spectral variability for many types of explosions and to the corrections for source and site terms; (3) path-specific corrections (e.g., using kriging) are very beneficial for extended regions, but they are not required to obtain good discrimination performance; and (4) source model comparisons are quite favorable at all of these test sites. Further understanding and source modeling work is needed.

ACKNOWLEDGMENTS

Seismic data from the IRIS DMC and the OHPDMC were used in this study.

REFERENCES

Brune, J. N. (1970). Tectonic stress and the spectra of seismic shear waves from earthquakes, *J. Geophys. Res.* 75: 4997–5009.

Fisk, M. D. (2006). Source spectral modeling of regional P/S discriminants at nuclear test sites in China and the Former Soviet Union, *Bull. Seism. Soc. Am*. 96: 2348–2367.

Fisk, M. D. (2007). Corner frequency scaling of regional seismic phases for underground nuclear explosions at the Nevada Test Site, *Bull. Seism. Soc. Am*. 97: 977–988.

Fisk, M. D. (2008). Enhancement and Modeling of Seismic Event Discrimination Based on Two-Dimensional Grids of Regional P/S Spectral Ratios, ATK-R-1741, ATK Technical Report.

Fisk, M. D. (2009). Seismic Event Discrimination for the Arctic Region using Two-Dimensional Grids of Regional P/S Spectral Ratios, ATK-R-1742, ATK Technical Report.

Fisk, M. D., H. L. Gray, and G. D. McCartor (1993). Applications of Generalized Likelihood Ratio Tests to Seismic Event Identification, PL-TR-93-2221, Phillips Lab., Hanscom AFB, MA.

Fisk, M. D. and G. D. McCartor (2008). Treatment of correlation for clustered reference data in kriging regional seismic discriminants, *Bull. Seism. Soc. Am*. 98: 1768–1780.

Fisk, M. D., S. R. Taylor, H. J. Patton, and W. R. Walter (2008). Applications of a next-generation MDAC discrimination procedure using two-dimensional grids of regional P/S spectral ratios, in *Proceedings of the 30th Monitoring Research Review: Ground-Based Nuclear Explosion Monitoring Technologies,* LA-UR-08-05261, Vol. 1, pp. 583–592.

Kim, W. Y., V. Aharonian, A. L. Lerner-Lam and P. G. Richards (1997). Discrimination of earthquakes and explosions in southern Russia using regional high-frequency three-component data from IRIS/JSP Caucasus Network, *Bull. Seism. Soc. Am.* 87: 569–588.

Kim, W. Y., and P. G. Richards (2007). North Korean nuclear test: seismic discrimination at low yield, *Eos* 88: 158–161.

Koper, K. D., R. B. Herrmann, and H. M. Benz (2008). Overview of open seismic data from the North Korea event of 9 October 2006, *Seism. Res. Lett.* 79: 178–185.

Mueller, C. S. and J. R. Murphy (1971). Seismic characteristics of underground nuclear detonations Part I: seismic spectrum scaling, *Bull. Seism. Soc. Am.* 61: 1675–1692.

Murphy, J. R., B. W. Barker, D. D. Sultanov, and O. P. Kuznetsov (2009). S-wave generation by underground explosions: implications from observed frequency-dependent source scaling, *Bull. Seism. Soc. Am.* 99: 809–829.

Taylor, S. R. (2009). Can the Fisk Conjecture be Explained by Rock Damage Around Explosions?, *Bull. Seism. Soc. Am.*, in press.

Taylor, S. R., A. A. Velasco, H. E. Hartse, W. S. Phillips, W. R. Walter, and A. J. Rodgers (2002). Amplitude corrections for regional seismic discriminants, *Pure Appl. Geophys.* 159: 623–650.

Walter, W. R., E. Matzel, M. E. Pasyanos, D. B. Harris, R. Gok, and S. R. Ford (2007). Empirical observations of earthquake-explosion discrimination using P/S ratios and implications for the sources of explosion S-waves, in *Proceedings of the 29th Monitoring Research Review: Ground-Based Nuclear Explosion Monitoring Technologies,* LA-UR-07-5613, Vol. 1, pp. 684–693.

Walter, W. M. E. Pasyanos, R., E. Matzel, R. Gok, J. J. Sweeney, S. R. Ford, and A. J. Rodgers (2008). Regional seismic amplitude modeling and tomography for earthquake-explosion discrimination, in *Proceedings of the 30th Monitoring Research Review: Ground-Based Nuclear Explosion Monitoring Technologies,* LA-UR-08-05261, Vol. 1, pp. 702– 711.

Xie, J. and H. J. Patton (1999). Regional phase excitation and propagation in the Lop Nor region of central Asia and implications for P/Lg discriminants, *J. Geophys. Res.* 104: 941–954.